

Modeling and Analysis of a Novel Variable-Speed Cage Induction Generator

Udaya K. Madawala, *Senior Member, IEEE*, Tobias Geyer, *Senior Member, IEEE*,
Jonathan B. Bradshaw, *Student Member, IEEE*, and D. Mahinda Vilathgamuwa, *Senior Member, IEEE*

Abstract—This paper introduces a novel cage induction generator and presents a mathematical model, through which its behavior can be accurately predicted. The proposed generator system employs a three-phase cage induction machine and generates single-phase and constant-frequency electricity at varying rotor speeds without an intermediate inverter stage. The technique uses any one of the three stator phases of the machine as the excitation winding and the remaining two phases, which are connected in series, as the power winding. The two-series-connected-and-one-isolated (TSCAOI) phase winding configuration magnetically decouples the two sets of windings, enabling independent control. Electricity is generated through the power winding at both sub- and super-synchronous speeds with appropriate excitation to the isolated single winding at any frequency of generation. A dynamic mathematical model, which accurately predicts the behavior of the proposed generator, is also presented and implemented in MATLAB/Simulink. Experimental results of a 2-kW prototype generator under various operating conditions are presented, together with theoretical results, to demonstrate the viability of the TSCAOI power generation. The proposed generator is simple and capable of both storage and retrieval of energy through its excitation winding and is expected to be suitable for applications, such as small wind turbines and microhydro systems.

Index Terms—Alternating-current (ac) generators, induction generators, self-excitation, standalone operation, wind power generation.

I. INTRODUCTION

THE use of renewable energy as an alternative to low-cost fossil energy, which was in abundance, has never been considered as an economically viable option in the past. However, the excessive, unnecessary, and inefficient use of fossil energy has now become a global concern, owing to rapidly decreasing fossil resources, rising fuel prices, increasing demand for energy, and, more importantly, the awareness of global warming and environmental impact. Consequently, it has now become a common practice of governing bodies to place more emphasis on energy saving, harnessing renewable energy, and particularly on energy management through efficient gener-

Manuscript received April 7, 2010; revised September 12, 2010, January 21, 2011, and March 20, 2011; accepted March 29, 2011. Date of publication May 19, 2011; date of current version October 18, 2011. This work was supported in part by the Faculty of Engineering Research and Development Fund at The University of Auckland and in part by Auckland Uniservices, Ltd.

U. K. Madawala, T. Geyer, and J. B. Bradshaw are with The University of Auckland, Auckland, 1020, New Zealand (e-mail: u.madawala@auckland.ac.nz).

D. M. Vilathgamuwa is with Nanyang Technological University, Singapore 639798.

Color versions of one or more of the figures in this paper are available online at <http://ieeexplore.ieee.org>.

Digital Object Identifier 10.1109/TIE.2011.2157277

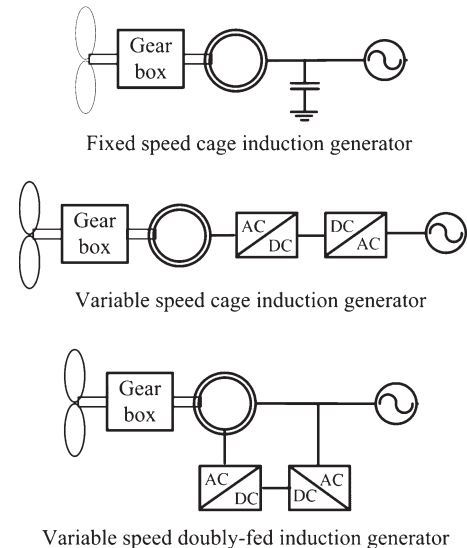


Fig. 1. Typical induction generator systems used in wind turbines.

ation, conversion, transmission, and distribution. This initiative incited a new area of active research and development within both academia and industry under the context of “green or clean or renewable” energy [1]–[3].

Mechanical-to-electrical energy conversion can be realized through a variety of techniques. These techniques vary from one to the other, owing to different levels of sophistication, characteristics, complexity, performance, cost, etc., and are suitable for a range of energy sources and applications from very low to very high power levels. Among the various renewable energy sources that are available, wind energy can be considered as a source that has been widely used. Wind turbine systems have been in use for power levels ranging from megawatts to microwatts, where miniature sensors are powered. In these wind turbine systems, various technologies have been employed to perform the mechanical-to-electrical energy conversion. Fig. 1 shows three electricity generation schemes, based on three phase induction generators, employed in typical wind turbine systems.

Of the schemes illustrated in Fig. 1, fixed-speed cage three-phase induction generators are well known for their simplicity and low cost and operated at constant rotor speed to generate electricity at constant frequency for both direct grid integration and standalone operation. Usually, they are excited through a bank of capacitors and are incapable of tracking maximum power that is available from the wind turbine when operated at constant speed [4]–[6]. Therefore, in order to extract maximum

energy under varying wind speed conditions, an intermediate power conversion stage, comprising an alternating-current (ac)/direct-current (dc) and dc/ac back-to-back converter configuration, is employed between the generator and the grid or the load [7]–[15]. The intermediate stage allows for the variable-speed operation of the generator, but it essentially requires to be rated for the same or a fraction (in the case of doubly fed induction generators) of the power level of the generator itself. Thus, such an intermediate stage is often found to be economically unjustifiable for some applications, particularly at micropower levels.

Induction generators have been also employed to generate single-phase electricity, particularly for standalone or residential use [16]–[18]. In [19] and [20], a self-excited and self-regulated single-phase induction generator has been reported for the generation of single-phase electricity. In contrast, the analysis of the self-excitation of a dual-winding induction generator has been presented in [21]. This paper, which uses a single-phase cage induction machine with an auxiliary winding, has been extended by connecting an inverter to the auxiliary winding to achieve more flexibility in power control [22]. All these reported schemes employed a single-phase induction generator and an auxiliary winding in some cases or a three-phase induction generator to generate single-phase electricity at constant or above synchronous speed.

In contrast with single-phase cage induction machines, three-phase cage induction machines are less expensive and small in size for a similar power rating. According to literature, a single-phase electricity generation scheme, based on a variable-speed three-phase cage induction machine without an intermediate inverter stage, is yet to be reported. This paper presents a novel technique [23], whereby a three-phase cage induction machine can be used as a single-phase generator under both sub- and super-synchronous variable-speed conditions without an intermediate inverter stage. The technique uses one of the three windings in isolation for excitation and the remaining two, which are connected in series, as the power winding for the single-phase electricity generation. Alternatively, the two series-connected windings may be also used for excitation while the power is generated through the isolated single winding, as detailed in [24]. The three-phase cage induction machine is mathematically modeled in the proposed two-series-connected-and-one-isolated (TSCAOI) phase winding configuration. The theoretical performance is investigated under varying operating conditions and compared with a prototype 2-kW single-phase electricity generator. Both simulated and experimental results are in good agreement and indicate that the machine can be operated both at sub- and super-synchronous rotor speeds to generate electricity at constant frequency. The proposed technique allows for both energy storage and retrieval through the excitation winding and is expected to gain popularity, particularly in small-scale applications, being relatively simple and low in cost.

II. PROPOSED NOVEL CAGE INDUCTION GENERATOR

Cage induction machines are undoubtedly the workhorse of the industry and can be still regarded as the main competitor

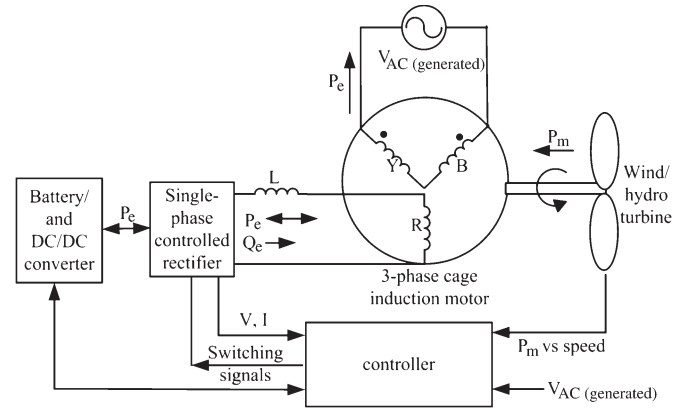


Fig. 2. Proposed generator in TSCAOI winding configuration.

to permanent-magnet machines. This is because they are self-starting, rugged, reliable, and efficient and offer a long trouble-free working life. Of these cage induction machines, three-phase machines are significantly less expensive, more efficient, and smaller in frame size in comparison with their single-phase counterpart of similar power ratings. Consequently, three-phase cage induction motors are economically more appealing and have thus become the preferred choice for numerous applications, even at derated power levels as encountered in the Steinmetz configuration [25], [26].

The novel technique proposed in this paper also uses a three-phase cage induction machine, exploiting its economical advantage, to generate single-phase electricity at variable rotor speeds without an intermediate inverter stage. The technique configures the three stator windings of the three-phase cage induction machine in a novel way to create separate or rather decoupled excitation and power windings. In this configuration, any one of the three phase windings is solely used in isolation for excitation, whereas the remaining two are connected in series to generate power at a desired frequency while the rotor is driven at any given speed. Alternatively, the machine can be also configured in such a way that the two series-connected windings provide the excitation while the single winding generates. The proposed TSCAOI winding configuration of a three-phase cage induction machine is shown in Fig. 2. As mathematically shown in the following section, the TSCAOI winding configuration magnetically decouples both excitation and power windings from each other and thus allows for independent control as in the case of a single-phase induction motor with an auxiliary winding.

In the proposed technique, excitation for the generator is provided through the single winding, which is powered by a battery using either a simple square-wave inverter or a controlled rectifier. The former is the simplest and can be operated at the desired generation frequency using a less sophisticated controller to provide the reactive-power requirement of the generator. In the latter case, as shown in Fig. 2, the system is relatively sophisticated but facilitates bidirectional power flow, allowing for both energy storage and later retrieval. The level of excitation in both cases is governed by the voltage generated in the power winding. A controller, comprising of a voltage feedback, can be employed to regulate the excitation. The

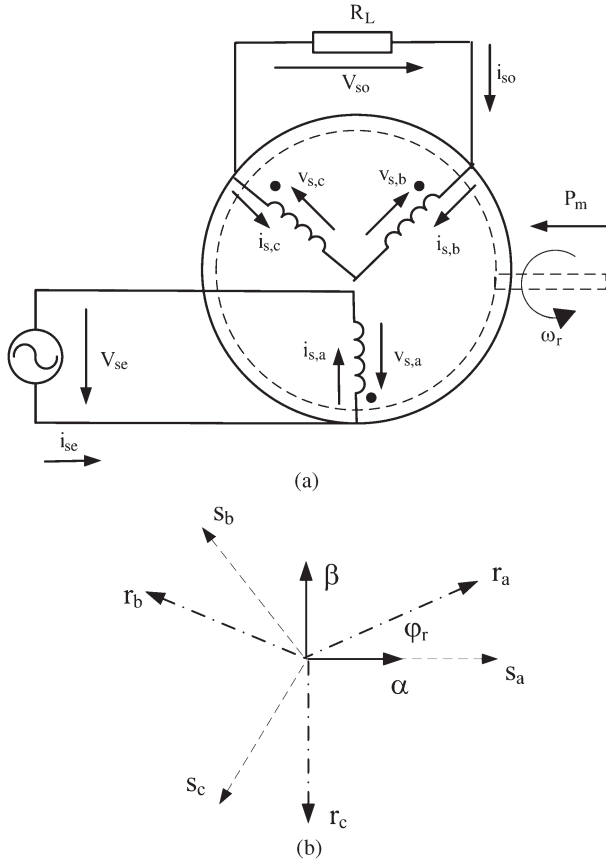


Fig. 3. (a) TSCAOI model and (b) stator and rotor with respect to the “ $\alpha\beta$ ” frame.

controller in the simplest form may provide only the reactive-power requirement of the generator (not the load) and, at a more sophisticated level, may be used to control both the active- and reactive-power flows in accordance with the phase angle and the voltage magnitude between the inverter and the excitation winding.

III. MATHEMATICAL MODEL

Fig. 3(a) shows a three-phase cage induction machine configured in the proposed TSCAOI winding arrangement with no closed-loop control. For the derivation of a model, it is assumed that the “ α ” axis of the “ $\alpha\beta$ ” frame is aligned with phase “a” of the stator windings, as shown in Fig. 3(b). If the rotor phase “a” is assumed to be at angle φ_r from the α axis, rotor quantities can be transformed into the “ $\alpha\beta$ ” frame using the following transformation:

$$[K_r] = \frac{2}{3} \begin{bmatrix} \cos(\varphi_r) & \cos(\varphi_r + \frac{2\pi}{3}) & \cos(\varphi_r - \frac{2\pi}{3}) \\ \sin(\varphi_r) & \sin(\varphi_r + \frac{2\pi}{3}) & \sin(\varphi_r - \frac{2\pi}{3}) \end{bmatrix}. \quad (1)$$

According to the TSCAOI configuration, the relationship between the voltages and the currents in the power and excitation windings and those in the stator-phase windings can be given by

$$[v_{s, eo}] = [Q][v_{s, abc}] \quad (2)$$

$$[i_{s, eo}] = [Q][i_{s, abc}] \quad (3)$$

where

$$[v_{s, eo}] = \begin{bmatrix} v_{se} \\ v_{so} \end{bmatrix} \quad [i_{s, eo}] = \begin{bmatrix} i_{se} \\ i_{so} \end{bmatrix} \quad [v_{s, abc}] = \begin{bmatrix} v_{sa} \\ v_{sb} \\ v_{sc} \end{bmatrix}$$

$$[i_{s, abc}] = \begin{bmatrix} i_{sa} \\ i_{sb} \\ i_{sc} \end{bmatrix} \quad [Q] = \begin{bmatrix} 1 & 0 & 0 \\ 0 & 1 & -1 \end{bmatrix} \quad [Q]^{-1} = [Q]^T.$$

A three-phase cage induction machine can be represented in the “abc” frame by the following standard equations:

$$[v_{s, abc}] = [R_s][i_{s, abc}] + p \{ [L_s][i_{s, abc}] \} + p \{ [L_{sr}][i_{r, abc}] \} \quad (4)$$

$$[v_{r, abc}] = [R_r][i_{r, abc}] + p \{ [L_{sr}]^T[i_{s, abc}] \} + p \{ [L_r][i_{r, abc}] \} \quad (5)$$

where p is the differential operator, $[v_{r, abc}]$ and $[i_{r, abc}]$ are defined according to $[v_{s, abc}]$ and $[i_{s, abc}]$, respectively, $[v_{r, abc}] = 0$ for cage machines, and

$$[R_s] = \begin{bmatrix} r_s & 0 & 0 \\ 0 & r_s & 0 \\ 0 & 0 & r_s \end{bmatrix} \quad [R_r] = \begin{bmatrix} r_r & 0 & 0 \\ 0 & r_r & 0 \\ 0 & 0 & r_r \end{bmatrix}$$

$$[L_s] = \begin{bmatrix} (L_{ls} + L_{ms}) & -L_{ms}/2 & -L_{ms}/2 \\ -L_{ms}/2 & (L_{ls} + L_{ms}) & -L_{ms}/2 \\ -L_{ms}/2 & -L_{ms}/2 & (L_{ls} + L_{ms}) \end{bmatrix}$$

$$[L_r] = \begin{bmatrix} (L_{lr} + L_{mr}) & -L_{mr}/2 & -L_{mr}/2 \\ -L_{mr}/2 & (L_{lr} + L_{mr}) & -L_{mr}/2 \\ -L_{mr}/2 & -L_{mr}/2 & (L_{lr} + L_{mr}) \end{bmatrix}$$

$$[L_{sr}] = L_{ms} \begin{bmatrix} \cos(\varphi_r) & \cos(\varphi_r + \frac{2\pi}{3}) & \cos(\varphi_r - \frac{2\pi}{3}) \\ \cos(\varphi_r - \frac{2\pi}{3}) & \cos(\varphi_r) & \cos(\varphi_r + \frac{2\pi}{3}) \\ \cos(\varphi_r + \frac{2\pi}{3}) & \cos(\varphi_r - \frac{2\pi}{3}) & \cos(\varphi_r) \end{bmatrix}.$$

In these equations, parameters r_s , r_r , L_{ls} , L_{ms} , L_{lr} , L_{mr} , and L_{sr} are the stator resistance, the rotor resistance, the stator leakage, the stator magnetization, the rotor leakage, the rotor magnetization, and the stator-to-rotor mutual inductance referred to the stator side, respectively. The stator and rotor parameters in the “abc” frame can be now transformed into the “eo” and “ $\alpha\beta$ ” frames, respectively, i.e.,

$$[v_{s, eo}] = [Q][R_s][Q]^{-1}[i_{s, eo}] + [Q]p \{ [L_s][Q]^{-1}[i_{s, eo}] \} + [Q]p \{ [L_{sr}][K_r]^{-1}[i_{r, \alpha\beta}] \} \quad (6)$$

$$[v_{r, \alpha\beta}] = [K_r][R_r][K_r]^{-1}[i_{r, \alpha\beta}] + [K_r]p \{ [L_{sr}]^T[Q]^{-1}[i_{s, eo}] \} + [K_r]p \{ [L_r][K_r]^{-1}[i_{r, \alpha\beta}] \}. \quad (7)$$

After lengthy manipulations with appropriate substitutions, (6) and (7) can be rewritten in the following form:

$$[v_{s, eo}] = r_s \begin{bmatrix} 1 & 0 \\ 0 & 2 \end{bmatrix} [i_{s, eo}] + \begin{bmatrix} L_{ls} + L_{ms} & 0 \\ 0 & 2L_{ls} + 3L_{ms} \end{bmatrix} p[i_{s, eo}] + \frac{3}{2} L_{ms} \begin{bmatrix} 1 & 0 \\ 0 & \sqrt{3} \end{bmatrix} p[i_{r, \alpha\beta}] \quad (8)$$

$$\begin{aligned}
0 &= L_{\text{ms}}\omega_r \begin{bmatrix} 0 & \sqrt{3} \\ -1 & 0 \end{bmatrix} [i_{s,\text{eo}}] \\
&+ L_{\text{ms}} \begin{bmatrix} 1 & 0 \\ 0 & \sqrt{3} \end{bmatrix} p[i_{s,\text{eo}}]r_r[i_{r,\alpha\beta}] \\
&+ \left(L_{\text{lr}} + \frac{3}{2}L_{\text{ms}} \right) \omega_r \begin{bmatrix} 0 & 1 \\ -1 & 0 \end{bmatrix} [i_{r,\alpha\beta}] \\
&+ \left(L_{\text{lr}} + \frac{3}{2}L_{\text{ms}} \right) p[i_{r,\alpha\beta}] \quad (9)
\end{aligned}$$

where ω_r is the rotor speed in electrical radians per second.

From (8) and (9), it is evident that the excitation and power windings are decoupled. To complete the machine model, it is necessary to select state variables and derive the appropriate equations for integration. In this case, the elements of the machine current vector are chosen as the state variables.

Equation (10) shows the state space model using the winding currents as the phase vector, as derived from (8) and (9), i.e.,

$$p[i] = [A][i] + [B][v] \quad (10)$$

where the parameters are shown at the bottom of the page.

The electromagnetic torque of the machine can be derived from

$$T_e = \frac{P}{2} [i_{s,\text{abc}}] \frac{\partial}{\partial \varphi_r} \{ [L_{\text{sr}}] [i_{r,\text{abc}}] \} \quad (11)$$

where P denotes the number of poles. Equation (11) in “abc” quantities is transformed into the “eo” and “ $\alpha\beta$ ” frames and can be given by

$$T_e = \frac{P}{2} L_M (\sqrt{3}i_{\text{so}}i_{r\alpha} - i_{\text{se}}i_{r\beta}). \quad (12)$$

Equation (12) represents the torque components due to both load and excitation currents. At the steady state, the torque

given in (12) is equal to the turbine torque. The equation of the motion of the generator is given by

$$p\omega_r = \frac{P}{2} \frac{1}{J} (T_P - T_e) \quad (13)$$

where J (in $\text{kg} \cdot \text{m}^2$) is the inertia and T_P (in nanometers) is the torque of the prime mover.

IV. CONTROL OF THE GENERATOR

Both the behavior and the performance of the machine in the proposed TSCAOI generator configuration are investigated through simulations, implementing the previously mentioned mathematical model in MATLAB/Simulink and experimentally using a 2-kW prototype generator. A standalone and resistive load is considered during the investigation. For each combination of the load resistance and the mechanical torque input, the excitation control system must supply reactive power to the generator in order to maintain the desired output voltage. Because the output power is fixed by the load in the standalone mode, the excitation inverter also serves as either a sink or a source for real power in order to balance the mechanical power input and the electrical load. Investigations of the open-loop behavior of the machine reveal two important characteristics. First, the output frequency of the machine is equal to the excitation frequency. Second, the magnitude of the output voltage is strongly dependent on the magnitude of the excitation voltage, which regulates the var requirement of the generator.

This information was used to develop the closed-loop controller, as shown in Fig. 4. The single-phase output voltage V_O is converted to a root-mean-square (RMS) value and compared with the desired output voltage, in this case, 230-V RMS. The voltage error is fed to a proportional–integral (PI) controller, which sets the excitation voltage magnitude $V_{E,\text{RMS}}$. Design aspects of the PI controller are discussed in Section V. The

$$\begin{aligned}
[i] &= [i_{\text{se}} \quad i_{\text{so}} \quad i_{r\alpha} \quad i_{r\beta}]^T & [v] &= [v_{s,\text{eo}}] = [v_{\text{se}} \quad v_{\text{so}}]^T \\
[A] &= \begin{bmatrix} -\frac{r_s L_{\text{rr}}}{D_1} & \frac{2L_M^2 \omega_r}{\sqrt{3}D_1} & \frac{L_M r_r}{D_1} & \frac{L_M L_{\text{rr}} \omega_r}{D_1} \\ -\frac{L_M^2 \omega_r}{\sqrt{3}D} & -\frac{r_s L_{\text{rr}}}{D} & -\frac{\sqrt{3}L_M L_{\text{rr}} \omega_r}{2D} & \frac{\sqrt{3}L_M r_r}{2D} \\ \frac{2r_s L_M}{3D} & -\frac{2L_M (L_{\text{ls}} + \frac{2}{3}L_M) \omega_r}{\sqrt{3}D} & -\frac{r_r (L_{\text{ls}} + \frac{2}{3}L_M)}{D} & -\frac{L_{\text{rr}} (L_{\text{ls}} + \frac{2}{3}L_M) \omega_r}{D} \\ \frac{2L_M L_{\text{ss}} \omega_r}{3D} & \frac{2r_s L_M}{\sqrt{3}D} & \frac{L_{\text{ss}} L_{\text{rr}} \omega_r}{D} & -\frac{L_{\text{ss}} r_r}{D} \end{bmatrix} \\
[B] &= \begin{bmatrix} \frac{L_{\text{rr}}}{D_1} & 0 \\ 0 & \frac{L_{\text{rr}}}{2D} \\ -\frac{2L_M}{3D} & 0 \\ 0 & -\frac{L_M}{\sqrt{3}D} \end{bmatrix} \\
L_M &= \frac{3}{2}L_{\text{ms}} & L_{\text{ss}} &= L_{\text{ls}} + L_M & L_{\text{rr}} &= L_{\text{lr}} + L_M \\
D &= (L_{\text{ss}} L_{\text{rr}} - L_M^2) \\
D_1 &= L_{\text{ls}} L_{\text{rr}} + \frac{2}{3}L_{\text{lr}} L_M
\end{aligned}$$

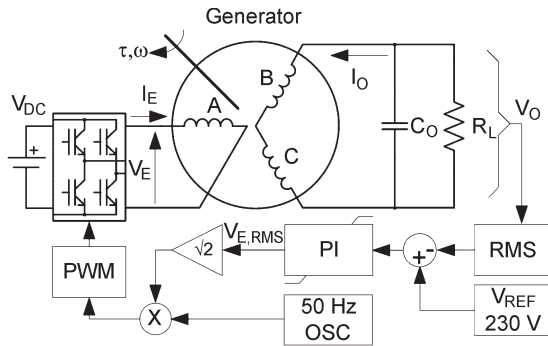


Fig. 4. Control block diagram.

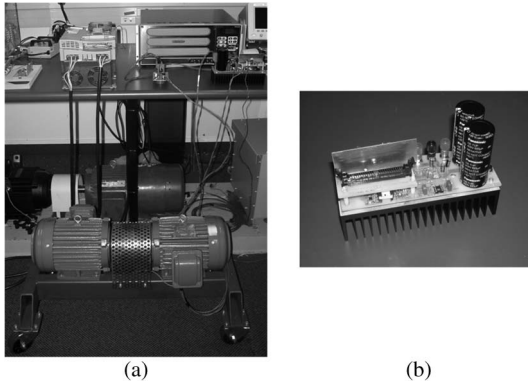


Fig. 5. (a) Experimental setup. (b) H-bridge inverter.

frequency of generation is set by a fixed-frequency 50-Hz oscillator, the output of which is multiplied with the excitation voltage reference to produce a sinusoidal control voltage for a full-bridge inverter. The inverter is connected to a 300-V dc bus V_{DC} and controlled using pulsewidth modulation at 5 kHz to produce the required excitation voltage. As mentioned earlier, depending on the mechanical input torque τ and load R_L , the inverter will either sink or source real power. The sinking of real power is facilitated by controlling the dc bus voltage using a chopper circuit and a dump resistor.

V. EXPERIMENTAL VERIFICATION

In order to demonstrate the practical viability of the proposed concept, a prototype 2-kW generator was built using a TECO four-pole 3-kW 400-V cage induction machine. The experimental setup is shown in Fig. 5, and the details of the cage induction machine are given in the Appendix. The 3-kW induction machine was configured in the TSCAOI winding arrangement and was driven by another induction motor using a variable-speed drive (VSD) to emulate the variable wind conditions. The controller in Fig. 4 was implemented in a dSPACE environment, and the prototype generator was controlled through an inverter, as shown in Fig. 5(b), to supply power to a standalone and electronic load at 230 V/50 Hz under varying rotor speeds. A 30- μ F capacitor, shown as C_0 in Fig. 4, was employed to reduce the reactive-power requirement of the excitation source and to keep the magnitude of the excitation current below the rated value of the machine.

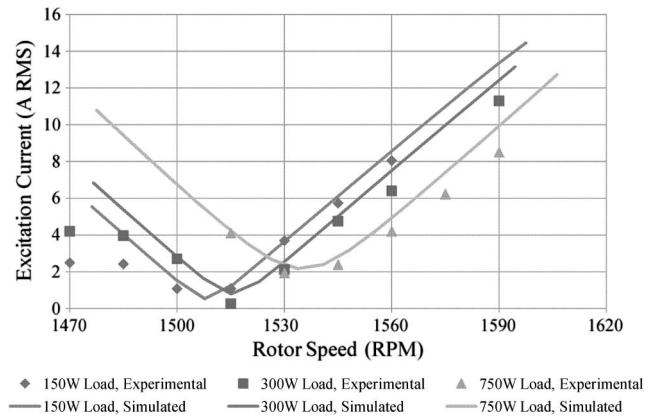


Fig. 6. Excitation current for different rotor speeds and loads.

Fig. 6 shows the variation of the excitation current for different rotor speeds of the generator and three different resistive loads. In all cases, the excitation control system presented in Fig. 4 is used to regulate the output voltage at 230-V RMS.

As evident, both experimental results and simulations are in agreement and exhibit the same trend. The small discrepancy can be attributed to some losses that have not been included in the mathematical model. It is interesting to note that, for each load, there exists a unique rotor speed, at which the excitation current is minimum. This is because the excitation source at this speed supplies only the reactive-power requirement of the generator as both the load power and the losses of the generator are met by the turbine. When the rotor speed is increased beyond this unique speed by increasing the torque setting of the VSD, the turbine power is increased, and the excess power is now absorbed by the excitation source, resulting in an increase in the excitation current. Similarly, when the rotor speed is reduced below the unique speed, the turbine power is supplemented by the excitation source, and as such, the excitation current increases. Below the synchronous speed of 50 Hz, the experimental results are rather constant in comparison with simulations. This is because the torque setting of the VSD could not be reduced below zero to further reduce the rotor speed. As a consequence, the rotational losses of the VSD drive (turbine) appear as a constant negative torque to the generator, which is solely run as a single-phase motor in this subsynchronous speed by the excitation winding.

The variation of the excitation voltage versus the rotor speed is shown in Fig. 7. The impedance seen by the excitation source is complex in nature, being dependent on both the excitation frequency and the slip frequency. The slip-frequency-dependent component of the impedance changes with the rotor speed and is therefore dictated by the rotor speed and current. It appears from results that the variation of both the excitation voltage and current is largely governed by the rotor-speed-dependent impedance, and therefore, the trend in the excitation voltage variation is expected to be similar to that observed for the excitation current, as shown in Fig. 6.

Fig. 8 demonstrates the variation of the real power of the excitation source for different rotor speeds. The negative power and the positive power indicate the power supplied and absorbed by the source, respectively. The rotor speed was simply

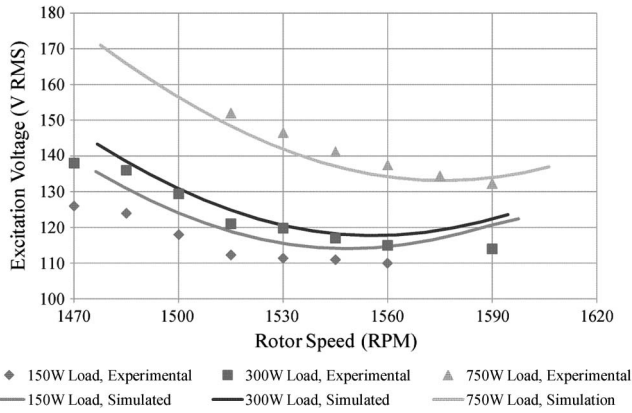


Fig. 7. Excitation voltage for different rotor speeds and loads.

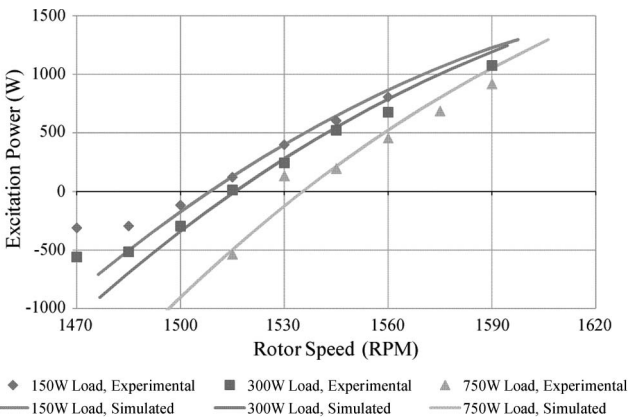


Fig. 8. Excitation power for different rotor speeds and loads.

increased or decreased by increasing or decreasing the torque setting of the VSD. It is clearly evident that, as described earlier, there is a unique rotor speed for each load at which the excitation source neither absorbs nor supplies real power but only meets the reactive-power requirement of the machine. At this speed, both the load power and the losses of the generator are met by the turbine and thus correspond to the minimum excitation current in Fig. 6. The operation of the generator above or below this rotor speed is similar to the operation of a doubly fed induction generator in the super- or subsynchronous mode, respectively. Above this rotor speed, the turbine power is more than that is required by the load and the losses of the generator, and hence, the excess power is absorbed by the excitation source. In contrast, the turbine is unable to meet the load power and the losses of the generator below this speed, and therefore, the excitation source supplements the turbine power. By adding the load power to the excitation power in Fig. 8, the total real electrical power output of the generator is obtained and shown in Fig. 9 with respect to varying rotor speeds. Both the experimental and simulated results are in good agreement except for speeds below the synchronous speed of 50 Hz. Below the synchronous speed, the torque setting of the VSD was set to zero to prevent regeneration and thus resulted in approximately constant experimental results in comparison with simulations, which were computed with a negative turbine torque.

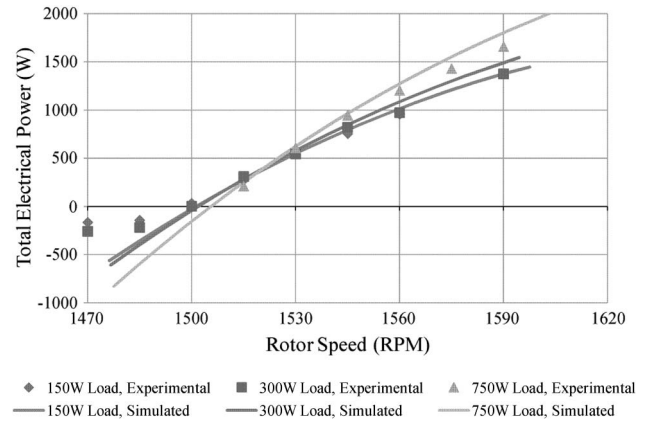


Fig. 9. Total electric power for different rotor speeds and loads.

The previously mentioned experimental results can be verified through approximate theoretical analysis. Assume that the machine is rated for P_{rated} at rated voltage V_L , current I_L , efficiency η , and power factor pf . Then

$$P_{rated} = \eta \sqrt{3} V_L I_L pf. \tag{14}$$

In the proposed configuration, power can be generated through both the excitation and power windings, whereas the var requirement of the machine is met by the excitation winding, supplemented by a capacitor connected to the power winding. This is because the total var requirement of the three-phase machine can never be met by the single excitation winding without exceeding its rated current, even at zero excitation real power. Under this condition, the maximum power P_{Gen} can be generated when both windings are generating power at rated voltage and current. If the power winding of the generator is connected to a resistive load and the generator operates at the same power factor, the generated power can be expressed by

$$P_{Gen} \approx [V_e I_e + V_o I_o] pf = \left[\frac{2}{\sqrt{3}} V_L I_L \right] pf. \tag{15}$$

Substituting (14) in (15)

$$P_{Gen} \approx \frac{2}{3\eta} P_{rated}. \tag{16}$$

Equation (16) thus suggests that approximately 2.3 kW can be generated from the 3-kW TECO machine used, which has an efficiency of 82%. It should be noted that the excitation voltage can never be as high as 230 V since the rated current should not be exceeded and the flux required to generate a line–line voltage of 230 V across the power winding is less. Therefore, factor 2 in (3) is slightly less and corresponds to an approximate output power of 2 kW.

The performance of the proposed generator was evaluated by measuring the efficiency for a range of output and excitation power levels, as shown in Fig. 10. A maximum efficiency of approximately 82% is observed when the output and excitation power levels are approximately equal.

The voltage and current waveforms of the output of the generator and the excitation source under different conditions are shown in Fig. 11. The situation, where the excitation

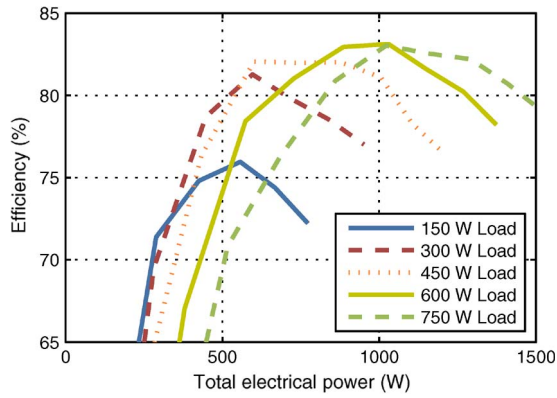


Fig. 10. Measured efficiency of the generator.

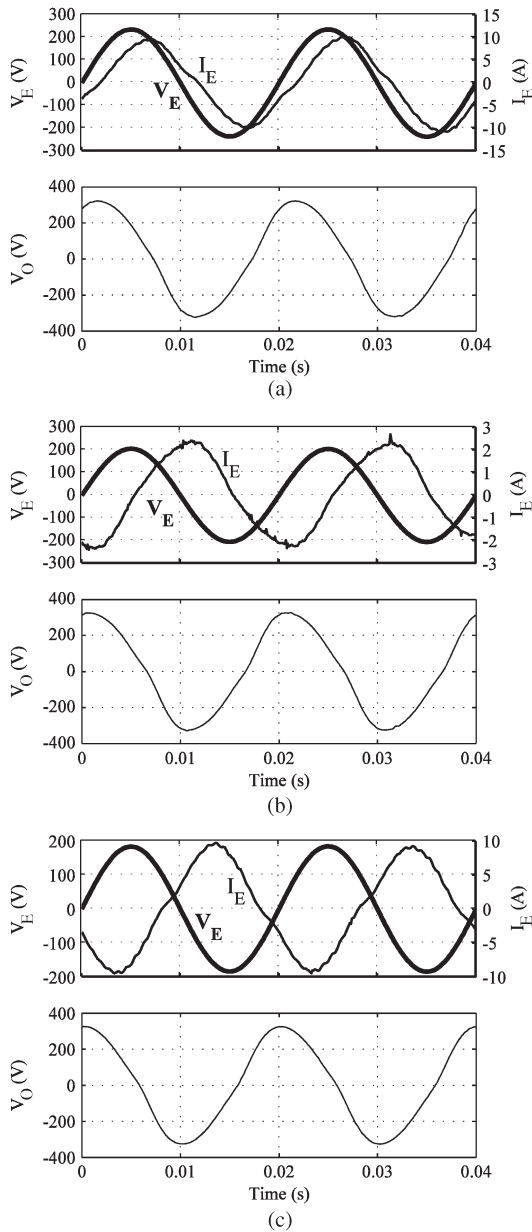


Fig. 11. Experimental waveforms of the output and the excitation source.

source provides both real power and reactive power to the generator, is demonstrated in Fig. 11(a). As evident from the waveforms of the excitation source, the phase angle between

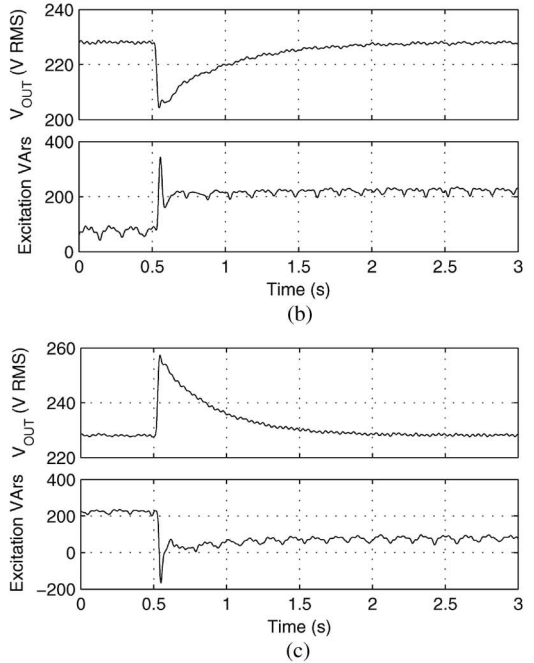
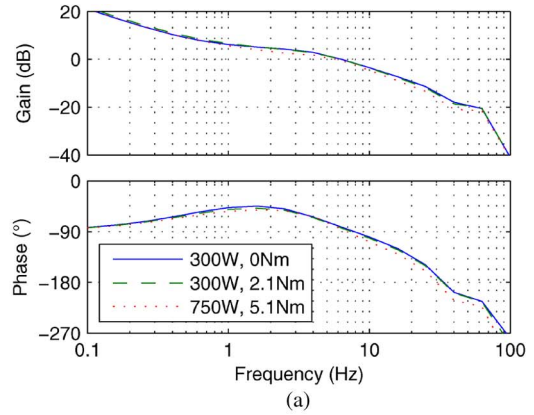


Fig. 12. (a) Bode plot and response of the controller for (b) an increase and (c) a reduction in the load.

the excitation voltage and current has settled to an angle, which is less than the ideal 90° , to cater for the active-power demand.

Fig. 11(b) shows the situation when the generator was operated at the speed at which the excitation current is minimum. As no real power was supplied by the excitation source at this speed, the phase angle is approximately 90° . As described earlier, at speeds where the turbine power exceeds load power, the excess real power is absorbed by the excitation source, and such an operation is demonstrated in Fig. 11(c).

Fig. 12 demonstrates how the proposed generator can be controlled under varying load conditions. Gains K_P and K_I of the controller proposed in Section IV were experimentally selected as 1 and 4, respectively, to deliver a reasonable settling time without overshoot. The simulated open-loop Bode plots of the machine at three different operating conditions are presented in Fig. 12(a). The three response curves are very similar, indicating that the controller is relatively robust, and the generator has a closed-loop bandwidth of approximately 6 Hz, with a phase margin of 110° and a gain margin of 17 dB.

The three curves were taken with fixed resistive load and turbine torque as shown. However, no attempt has been made to optimize the performance of the controller, being outside the scope of this paper.

Fig. 12(b) shows the output voltage and the reactive power supplied by the excitation source when the generator is subjected to an increase in the load at approximately 0.5 s. Obviously, the load voltage drops as the current reactive-power supply is inadequate to support the required output voltage, but the controller quickly responds and injects more reactive power to the generator, restoring its output voltage. Similarly, Fig. 12(c) illustrates a situation when the generator is subjected to reduction in the load at approximately 0.5 s. As expected, an increase in the load voltage is observed, but it is restored to its original value by reducing the amount of reactive power injected into the generator.

VI. CONCLUSION

A novel winding configuration that facilitates the generation of single-phase electricity from standard three-phase cage induction machines at variable speeds has been described, and a mathematical model, which predicts its behavior, has been also presented. The validity of the proposed concept of generation has been verified using simulations and experimental evidence of a prototype 2-kW generator. Both simulations and measured results indicate that the technique is viable and allows for the generation of electricity at constant frequency while the cage induction machine is operated at both sub- and super-synchronous speeds. The proposed generator is easy to implement and low in cost. It can be used for both energy storage and retrieval through its excitation winding, and it is an ideal candidate for small-scale renewable energy applications.

APPENDIX

Generator: A cage-type 3-kW TECO four-pole 400-V/50-Hz induction motor, which has the following parameters:

$$R_s = 1.5 \Omega$$

$$R_r = 2 \Omega$$

$$L_{ls} = 0.011 \text{ H}$$

$$L_{lr} = 0.011 \text{ H}$$

$$L_M = 0.214 \text{ H}$$

$$J = 0.01 \text{ kg} \cdot \text{m}^2.$$

REFERENCES

- [1] J. M. Guerrero, F. Blaabjerg, T. Zhelev, K. Hemmes, and K. Monmasson, "Distributed generation: Toward a new energy paradigm," *IEEE Ind. Electron. Mag.*, vol. 4, no. 1, pp. 52–64, Mar. 2010.
- [2] J. M. Carrasco, L. G. Franquelo, J. T. Bialasiewicz, and E. Galvan, "Power electronics systems for the grid integration of renewable energy sources: A survey," *IEEE Trans. Ind. Electron.*, vol. 53, no. 4, pp. 1002–1016, Jun. 2006.
- [3] C. Liu, K. T. Chau, and X. Zhang, "An efficient wind-photovoltaic hybrid generation system using doubly excited permanent magnet brushless dc machine," *IEEE Trans. Ind. Electron.*, vol. 57, no. 3, pp. 831–839, Mar. 2010.
- [4] G. Poddar, A. Joseph, and A. K. Unnikrishnan, "Sensorless variable-speed controller for existing fixed-speed wind power generator with unity-power-factor operation," *IEEE Trans. Ind. Electron.*, vol. 50, no. 5, pp. 1007–1015, Oct. 2003.
- [5] E. G. Marra and J. A. Pomilio, "Induction generator based system providing regulated voltage with constant frequency," *IEEE Trans. Ind. Electron.*, vol. 47, no. 4, pp. 908–914, Aug. 2000.
- [6] L. W. Li, G. Joos, and J. Belanger, "Real-time simulation of a wind turbine generator coupled with a battery supercapacitor energy storage system," *IEEE Trans. Ind. Electron.*, vol. 57, no. 4, pp. 1137–1145, Apr. 2010.
- [7] J. Lopez, E. Gubia, E. Olea, J. Ruiz, and L. Marroyo, "Ride through of wind turbines with doubly fed induction generator under symmetrical voltage dips," *IEEE Trans. Ind. Electron.*, vol. 56, no. 10, pp. 4246–4254, Oct. 2009.
- [8] B. C. Rabelo, W. Hofmann, J. L. da Silva, R. G. de Oliveira, and S. R. Silva, "Reactive power control design in doubly fed induction generators for wind turbines," *IEEE Trans. Ind. Electron.*, vol. 56, no. 10, pp. 4154–4162, Oct. 2009.
- [9] R. Takahashi, H. Kinoshita, T. Murata, J. Tamura, M. Sugimasa, A. Komura, M. Futami, M. Ichinose, and K. Ide, "Output power smoothing and hydrogen production by using variable speed wind generators," *IEEE Trans. Ind. Electron.*, vol. 57, no. 2, pp. 485–493, Feb. 2010.
- [10] G. O. Cimuca, C. Saudemont, B. Robyns, and M. M. Radulescu, "Control and performance evaluation of a flywheel energy-storage system associated to a variable-speed wind generator," *IEEE Trans. Ind. Electron.*, vol. 53, no. 4, pp. 1074–1085, Jun. 2006.
- [11] R. C. Bansal, "Three phase self excited induction generators: Overview," *IEEE Trans. Energy Convers.*, vol. 20, no. 2, pp. 292–299, Jun. 2005.
- [12] J.-C. Wu, "Novel circuit configuration for the compensation for the reactive power of induction generator," *IEEE Trans. Energy Convers.*, vol. 23, no. 1, pp. 156–162, Mar. 2008.
- [13] B. Singh, S. S. Murthy, and S. Gupta, "STATCOM based voltage regulator for self-excited induction generator feeding non-linear loads," *IEEE Trans. Ind. Electron.*, vol. 53, no. 5, pp. 1437–1452, Oct. 2006.
- [14] A. K. Jain and V. T. Ranganathan, "Wound rotor induction generator with sensorless control and integrated active filter for feeding non-linear load in stand-alone grids," *IEEE Trans. Ind. Electron.*, vol. 55, no. 1, pp. 218–228, Jan. 2008.
- [15] L. Xu, D. Zhi, and B. W. Williams, "Predictive current control of doubly-fed induction generators," *IEEE Trans. Ind. Electron.*, vol. 56, no. 10, pp. 4143–4153, Oct. 2009.
- [16] T. F. Chan and L. L. Lai, "Single phase operation of a three-phase induction generator using a novel line current injection method," *IEEE Trans. Energy Convers.*, vol. 22, no. 3, pp. 798–799, Sep. 2007.
- [17] T. F. Chan and L. L. Lai, "Capacitance requirement of a three-phase induction generator self-excited with a single capacitance and supplying a single load," *IEEE Trans. Energy Convers.*, vol. 17, no. 1, pp. 90–94, Mar. 2002.
- [18] T. F. Chan, "Performance analysis of a three-phase induction generator connected to a single phase power system," *IEEE Trans. Energy Convers.*, vol. 13, no. 3, pp. 205–213, Sep. 1998.
- [19] S. S. Murthy, "A novel self-excited self-regulated single phase induction generator—Part 1," *IEEE Trans. Energy Convers.*, vol. 8, no. 3, pp. 377–382, Sep. 1993.
- [20] L. Shridar, B. Singh, and S. S. Murthy, "Selection of capacitors for self regulated short shunt self excited induction generator," *IEEE Trans. Energy Convers.*, vol. 10, no. 1, pp. 10–17, Mar. 1995.
- [21] O. Ojo and I. Bhat, "An analysis of single phase self excited induction generators," *IEEE Trans. Energy Convers.*, vol. 10, no. 2, pp. 254–260, Jun. 1995.
- [22] O. Ojo, O. Omozusi, and A. A. Jimoh, "The operation of inverter assisted single phase induction generator," *IEEE Trans. Ind. Electron.*, vol. 47, no. 3, pp. 632–640, Jun. 2000.
- [23] U. K. Madawala, "An electrical generator," New Zealand Patent 563196, Jan. 29, 2009.
- [24] U. K. Madawala, T. Geyer, J. Bradshaw, and D. M. Vilathgamuwa, "A model for a novel induction generator," in *Proc. IEEE IECON*, Nov. 3–5, 2009, pp. 64–69.
- [25] S. E. M. De Oliveira, "Operation of three phase induction motors connected to one phase supply," *IEEE Trans. Energy Convers.*, vol. 5, no. 4, pp. 713–718, Dec. 1990.
- [26] C. A. Baguley and U. K. Madawala, "The impact of circuit variables on the starting performance of field aligned starting," *IEEE Trans. Ind. Electron.*, vol. 56, no. 6, pp. 2067–2075, Jun. 2009.



Udaya K. Madawala (M'95–SM'06) received the B.Sc. degree in electrical engineering (Hons.) from the University of Moratuwa, Moratuwa, Sri Lanka, in 1987 and the Ph.D. degree in power electronics from The University of Auckland, Auckland, New Zealand, in 1993.

Since 1997, he has been with the Department of Electrical and Computer Engineering, The University of Auckland, where he is currently an Associate Professor. His research interests are in the fields of power electronics, inductive power transfer, and

renewable energy.

Dr. Madawala is an active IEEE volunteer and serves as an Associate Editor for the IEEE TRANSACTION ON INDUSTRIAL ELECTRONICS and the IEEE TRANSACTION ON POWER ELECTRONICS. He is the Chairman of the IEEE Industrial Electronics Chapter in New Zealand and a member of the Power Electronics Technical Committee of the IEEE Industrial Electronics Society.



Tobias Geyer (M'08–SM'10) received the Dipl.-Ing. and Ph.D. degrees in electrical engineering from Eidgenössische Technische Hochschule Zurich, Zurich, Switzerland, in 2000 and 2005, respectively.

From 2006 to 2008, he was a Project Leader with the GE Global Research Center, Munich, Germany, working on control and modulation schemes for large medium-voltage electrical drives. Since late 2008, he has been with the Department of Electrical and Computer Engineering, The University of Auckland, Auckland, New Zealand, where he is currently a Senior Research Fellow. His research interests are in the intersection of power electronics, modern control theory, and mathematical optimization. This includes medium-voltage electrical drives, direct-current (dc)–dc power conversion, model predictive control, and switched linear (hybrid) systems.

Dr. Geyer was a recipient of the Second Prize Paper Award at the 2008 IEEE Industry Applications Society Meeting.



Jonathan B. Bradshaw (S'08) received the B.E. degree in electrical and computer engineering (First Class Hons.) in 2006 from The University of Auckland, Auckland, New Zealand, where he is currently working toward the Ph.D. degree on the bit-stream control of doubly fed induction generators since 2007.

He worked in the industry as a Power Systems Consultant, specializing in dynamic modeling and protective earthing. His research interests include power electronics and electrical machinery.



D. Mahinda Vilathgamuwa (S'90–M'93–SM'99) received the B.Sc. degree in electrical engineering from the University of Moratuwa, Moratuwa, Sri Lanka, in 1985 and the Ph.D. degree in electrical engineering from Cambridge University, Cambridge, U.K., in 1993.

In 1993, he was a Lecturer with the School of Electrical and Electronic Engineering, Nanyang Technological University, Singapore, where he is currently an Associate Professor. His current research interests include power electronic converters,

electrical drives, and power quality.

Dr. Vilathgamuwa is the Vice Chairman of the IEEE Section, Singapore, and a member of the Power Electronics Technical Committee for the Industrial Electronics Society.